Electrochimica Acta 202 (2016) 231–242

Contents lists available at ScienceDirect

Electrochimica Acta

journal homepage: www.elsevier.com/locate/electacta

Phosphate ions as effective inhibitors for carbon steel in carbonated solutions contaminated with chloride ions

L. Yohai[1,a], W. Schreiner[b], M. Vázquez[1,a,*], M.B. Valcarce[a]

[a] División Electroquímica y Corrosión, Facultad de Ingeniería, UNMdP—INTEMA, CONICET, J. B. Justo 4302, B7608FDQ Mar del Plata, Argentina
[b] Laboratório de Superfícies e Interfases, Departamento de Física, Universidade Federal do Paraná, 81531-990 Curitiba, PR, Brazil

ARTICLE INFO

Article history:
Received 27 August 2015
Received in revised form 21 October 2015
Accepted 26 October 2015
Available online 30 October 2015

Keywords:
Phosphate
Inhibitors
Chloride
Steel
Carbonated concrete

ABSTRACT

This investigation focuses on sodium biphosphate (Na_2HPO_4) as corrosion inhibitor for construction steel. All the tests are carried out in a solution that simulates the composition of the pores in chloride-contaminated carbonated concrete. The carbonated solution (CS) contained Na_2CO_3 (0.0015 mol L^{-1}), $NaHCO_3$ (0.03 mol L^{-1}) and NaCl (0.1 mol L^{-1}), resulting in $[Cl^-]/[OH^-]$=10000. Inhibited solutions (IS20, IS60 and IS100) incorporated 20, 60, and 100 mmol L^{-1} Na_2HPO_4 respectively. These were labeled IS20, IS60 and IS100 respectively and result in $[HPO_4^{2-}]/[Cl^-]$ = 0.2, 0.6, and 1. Cyclic voltammograms and anodic polarization curves were complemented with micro-Raman spectroscopy and XPS, to evaluate the surface film composition. The results show that chloride contamination promotes active corrosion. When phosphate ions are incorporated, steel becomes passive with a more positive corrosion potential (Ecorr), and pitting presents as the predominant form of localized corrosion. Raman spectra show a broad band, centred in 982 cm^{-1}, suggesting that phosphates incorporate to the passive film. Phosphates are also present in the corrosion products. The surface film becomes more protective to pitting for the highest biphosphate content. However, after pitting no repassivation was detected. After over one month in immersion, steel remains passive in the condition IS100, with inhibition efficiency higher than 99%. In contrast, in the case of IS60 and IS20, pitting was detected.

It can be concluded that phosphate ions are good candidates to be used as corrosion inhibitors for steel in chloride-contaminated concrete.

1. Introduction

Reinforced concrete is known to have excellent structural and durability properties. However, one of the main pathologies affecting the performance of reinforced concrete structures is the corrosion of the steel reinforcement bars (rebars).

In normal service conditions, the high alkalinity provided by concrete guarantees the presence of an oxide layer that protects steel against active corrosion. However, rebar corrosion may be triggered by external factors such as concrete acidification due to CO_2 diffusion, the presence of aggressive ions (mainly chlorides), or even more by a combination of these factors [1]. In constructions located close to the seashore, chloride ions penetrate the porous structure of concrete and reach the steel. Also, in many coastal cities in Argentina, the use of chloride-contaminated aggregates and water constitutes a recurrent malpractice [2].

The investigation of rebar corrosion is particularly challenging because concrete is a highly resistive and porous material. Frequently, the chemical environment present in the concrete pores is simulated using appropriate solutions [3,4]. Some authors have used highly carbonated solutions to carry out corrosion studies [5,6]. However, the real pore solution presents a low concentration of soluble carbonate and bicarbonate ions [7].

Inhibitors are frequently used to minimize the risk of rebar corrosion [8–10]. The probability of undergoing corrosion at a given chloride content is usually evaluated in terms of the chloride/hydroxyl ratio [11]. Alternatively, in the presence of chloride, inhibiting agents are evaluated as a function of the inhibitor/chloride ratio [12,13].

Several inorganic anions have been successfully used to inhibit the corrosion of steel in concrete, such as chromates, nitrites, tungstates and molybdates [14]. Compared to alternative inhibiting agents, the main advantages of phosphates are low cost and low toxicity. They can be used to pre-treat the rebars or can be admixed into concrete [15–17]. The beneficial effect of phosphate

* Corresponding author at: División Electroquímica y Corrosión, Facultad de Ingeniería, Universidad Nacional de Mar del Plata, INTEMA, CONICET Juan B. Justo 4302—B7608FDQ Mar del Plata, Argentina. Fax: +54 223 481 0046.
E-mail address: mvazquez@fi.mdp.edu.ar (M. Vázquez).
[1] ISE active member.

http://dx.doi.org/10.1016/j.electacta.2015.10.167
0013-4686/

has been attributed to their absorption onto the passive layer, thus displacing chlorides and hindering the initiation of localized corrosion [6]. Yet, the inhibition mechanism is somewhat controversial. Some authors consider that phosphates are anodic inhibitors, being effective only in the presence of oxygen. Other authors suggest that they act as cathodic inhibitors [16] while they behave as mixed inhibitors for $[PO_4^{3-}]/[Cl^-]$ ratios higher than 0.6 [13].

In this work, the effectiveness of sodium biphosphate as corrosion inhibitor has been tested in low carbonated solutions (pH=9) that simulate concrete pores contaminated with chlorides. The composition of the surface films formed in the presence of the contaminant, with and without the inhibitor will be discussed.

2. Experimental

2.1. Electrodes preparation

Steel electrodes were prepared from reinforcement bars with the following composition: Mn 0.635 wt%, C 0.299 wt%, Si 0.258 wt %, Cu 0.227 wt% and others impurities 0.245 wt%. Discs were cut, flattened and included in fast curing acrylic resin using polyvinyl chloride (PVC) holders. The geometrical area exposed was 0.503 cm^2. Each sample was provided with an appropriate electrical contact. Finally, the samples were abraded up to grade 1000 with emery paper and rinsed gently with distilled water.

2.2. Electrolyte composition

The electrolyte consisted of a carbonated solution (CS) prepared with a low content of carbonate ions to simulate the composition of the acidified solution present in the pores of carbonated concrete. CS contained Na_2CO_3 (0.0015 mol L^{-1}) and $NaHCO_3$ (0.03 mol L^{-1}), so that $[HCO_3^-] + [CO_3^{2-}] = 0.0315$ mol L^{-1} and pH = 9 [12]. To simulate a carbonated concrete that is also contaminated with chloride ions, CS incorporated 0.1 mol l^{-1} NaCl, resulting in $[Cl^-]/[OH^-]$=10000.

To evaluate the inhibitor effect, inhibiting solutions (IS) were prepared as described above and incorporated 20, 60, and 100 mmol L^{-1} Na_2HPO_4 [16,18]. These were labeled IS20, IS60 and IS100 respectively and result in $[HPO_4^{2-}]/[Cl^-]$ = 0.2, 0.6, and 1 with pH = 9 in every case.

All the experiments were carried out at room temperature (20 ± 2 °C) without stirring.

2.3. Electrochemical techniques

A conventional three-electrode cell was employed, together with a Voltalab PGZ 100 potentiostat. A Hg/HgO electrode with 1 mol L^{-1} KOH solution (MOE, E = 0.123 V vs. SHE) was used as reference. All the potentials will be referred to this electrode. The counter electrode was a platinum wire of large area. All tests were done without stirring.

Cyclic voltammograms were recorded after having deaerated the electrolyte by bubbling N_2 during 15 min. The electrodes were pre-treated in either CS or IS, holding them at –1.1 V_{MOE} for 5 min. Then the potential was scanned at 10 mV s^{-1} starting at −1.1 V_{MOE} and reversing the sweep at convenient values.

The corrosion potential (E_{corr}) was found to reach a stable value after 24 h in each condition. Polarization resistance (Rp), polarization curves and electrochemical impedance spectra were recorded after having kept the electrodes for 24 h at E_{corr} without deaereating.

Polarization resistance (R_p) was evaluated as $\Delta V/\Delta i$, from potential sweeps scanning ± 15 mV from the corrosion potential (E_{corr}) at a scan rate of 0.1 mV s^{-1}.

Electrochemical impedance spectroscopy (EIS) tests were performed at E_{corr} in each solution. The amplitude of the AC signal was ± 0.01 Vrms while the frequency was varied between 20 kHz and 1 mHz. The results were fitted to two equivalent circuits (see Fig. 1). Circuit **a** is the well-known Randles circuit while circuit **b** is typical of oxidized metals [12,19]. ZView™ [20] was used to fit the experimental data.

To record the anodic and cathodic polarization curves, the potentiodynamic scan was started at the E_{corr}, with a sweep rate of 0.1 mV s^{-1}.

2.4. Ex-situ Raman spectra

Raman spectra were recorded using an Invia Reflex confocal Raman microprobe with Ar^+ laser of 514 nm in backscattering mode, with a laser spot diameter of 10 μm at a power of 25 mW. A 50 X objective and an exposure time of 50 s (3 accumulations) were used. Raman spectra were collected on spots of interest after having subjected the electrodes to anodic polarization curves and weight loss tests. The samples were withdrawn and dried under N_2 atmosphere, and immediately transferred to the Raman chamber. The spectra were observed to be reproducible.

2.5. Weight loss determinations

The weight loss method was applied following the guidelines in ASTM D 2688 Standard Test Methods for Corrosivity of Water in the Absence of Heat Transfer. Disks having 5.67 cm^2 as geometrical area were cut and abraded to grade 120 with emery paper. Three weighted coupons were immersed in each test solutions (CS, IS20, IS60 and IS100) for 42 days. The containers were kept at room temperature in aerated conditions. For surface characterization, one coupon of each condition was conveniently dried to perform *ex-situ* Raman spectra. Then, the corrosion products were stripped by immersion in HCl 1 mol L^{-1}. Later the coupons were neutralized and rinsed, first with a saturated Na_2CO_3 solution and then with distilled water, to be finally dried and reweighted.

3. Results and discussion

3.1. Cyclic voltammograms

Fig. 2 shows the first cycle of voltammograms carried out in CS and IS100. A voltammogram recorded in alkaline solution without chloride ions contamination (AS, pH=13) is also included for the sake of comparison. The peaks present in this last voltammogram were discussed in detail elsewhere [13]. In this alkaline electrolyte, the passive region extends up to 0.6 V.

In contrast, in the carbonated solution CS, steel is in active dissolution, as the current increases steadily with the applied potential. The concentration of carbonate and bicarbonate ions is not high enough to develop a passive layer of $FeCO_3$ [1]. Mao and col. [21] reported that the concentration of bicarbonate ions should

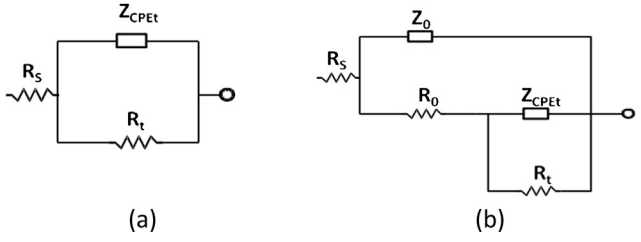

Fig. 1. Equivalent circuits chosen to fit EIS data. Circuit **a** is a typical Randles circuit and **b** is a circuit typically used to fit the behavior of oxide-coated metals.

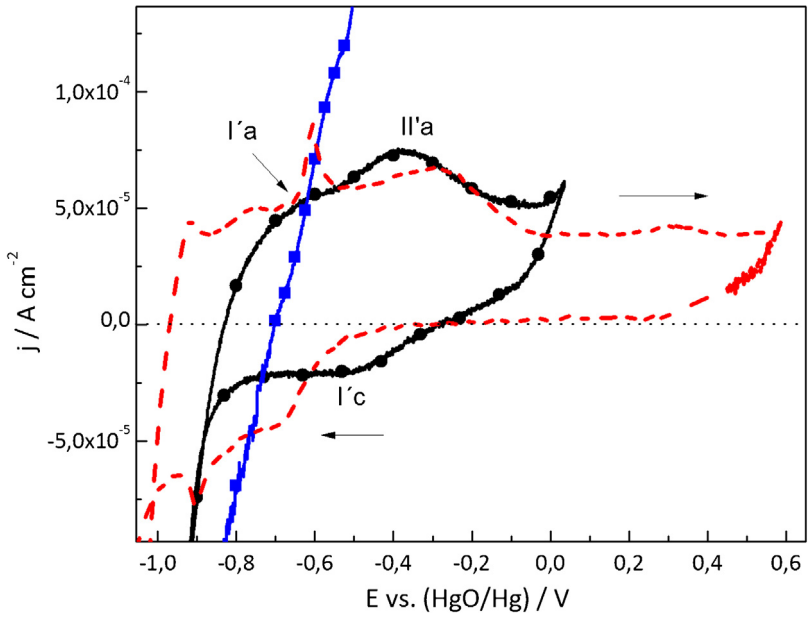

Fig. 2. Cyclic voltammograms of carbon steel recorded in CS (—■—), IS100 (—●—) and AS (— — —). Sweep rate: 10 mV s^{-1}.

be higher than 0.05 mol L^{-1} to guarantee steel passivation. The reactions below are clearly favored by high pH and by high contents of bicarbonate ions:

$$Fe + 2\ OH^- \rightarrow Fe(OH)_2 + 2e^- \quad (1)$$

$$Fe + HCO_3^- + OH^- \rightarrow FeCO_3 + H_2O + 2e^- \quad (2)$$

When HPO_4^{2-} ions are incorporated (solution IS100), the voltammogram shows two anodic peaks at -0.64 V (I'a) and at a -0.37 V (II'a) together with one cathodic peak (I'c) at -0.5 V. At potentials higher than 0.05 V, steel undergoes localized corrosion. Peaks I'a and II'a could be associated to Fe(II) and Fe(III) compounds [22]. Some authors have suggested that the surface film is composed by a mixture of iron oxides and ferrous phosphate [18] while others propose that only $Fe_3(PO_4)_2$ is present in the film [23]. In contrast, Genin and col. [24] argue that the simultaneous presence of phosphate ions and oxygen favors the oxidation of Fe^{2+} to Fe^{3+}, promoting γ-Fe_2O_3 formation in the surface film. According to Simpson and Melendres [25], Fe^{3+} oxides and oxohydroxides are less soluble than those of Fe^{2+} and contribute to the consolidation of a more stable passive film.

3.2. Corrosion potentials

The corrosion potential stabilized after 24 h immersion in each solution and the results are presented in Table 1. Values close to -500 mV are typical of actively corroding steel, which is the case for steel in CS. In the presence of the inhibiting agent, the values move in the positive direction. The most positive values correspond to the highest biphosphate content: $[HPO_4^{2-}]/[Cl^-] = 1$. This behavior suggests that biphosphates behave as anodic inhibitors when present in carbonated solutions with low carbonate content.

Table 1
Corrosion potentials and polarization resistance values measured after 24 h of immersion.

	E_{corr} vs. (Hg/HgO) / mV	R_P / kΩ cm^2
CS	-498 ± 51	1.26 ± 0.26
IS20	-238 ± 42	non linear response
IS60	-91 ± 6	non linear response
IS100	-17 ± 7	non linear response

3.3. Polarization resistance

Polarization resistance results measured after 24 h stabilization at E_{corr} are presented in Table 1. In the CS, values lower than 10 kΩ cm^2 confirm that steel is undergoing active dissolution. Similar results have been observed before by other authors [26,27]. When phosphates are present in solution, the relationship between current and potential is no longer lineal in the vicinity of the corrosion potential. Also, there is no coincidence between the potential at zero current and the corrosion potential. Fig. 3a and 3b compare the responses in the absence and presence of inhibitor. No clear value for the polarization resistance can be given when phosphates are present. This behavior has been reported before and attributed to various reasons [28]. Some authors argue that the deviation from linearity is caused by anodic and cathodic Tafel slopes with dissimilar values [29]. Kouril et al. [30], proposed that deviations happen when, after the initial jump in potential at the beginning of the potential sweep, the system needs time to reach the steady-state. The extent of the non-linearity is given by the capacitance of the electrode double-layer [31]. These deviations can be convenient to distinguish between a passive electrode and one actively corroding. This distinction relies on a simple method based on the linear regression of current-potential data. The coefficient of determination (R^2) quantifies these deviations and can be plotted against the difference between the corrosion potential and the potential at zero current ($E_{i=0}$ - E_{corr}). This representation is shown in Fig. 4. The data can be seen in different regions of the graphs. The group of points where ($E_{i=0}$ - E_{corr}) approaches zero with R tending to 1 corresponds to active dissolution (CS) while when the electrode is passive (IS) absolute values of ($E_{i=0}$ - E_{corr}) increase and R deviate from 1.

3.4. Polarization curves

Fig. 5 shows anodic polarization curves on electrodes that had been kept for 24 h at the E_{corr} in each solution. Table 2 presents relevant electrochemical parameters such as passivity currents (*j*pas), pitting potentials (E_{pit}) and the difference between E_{pit} -

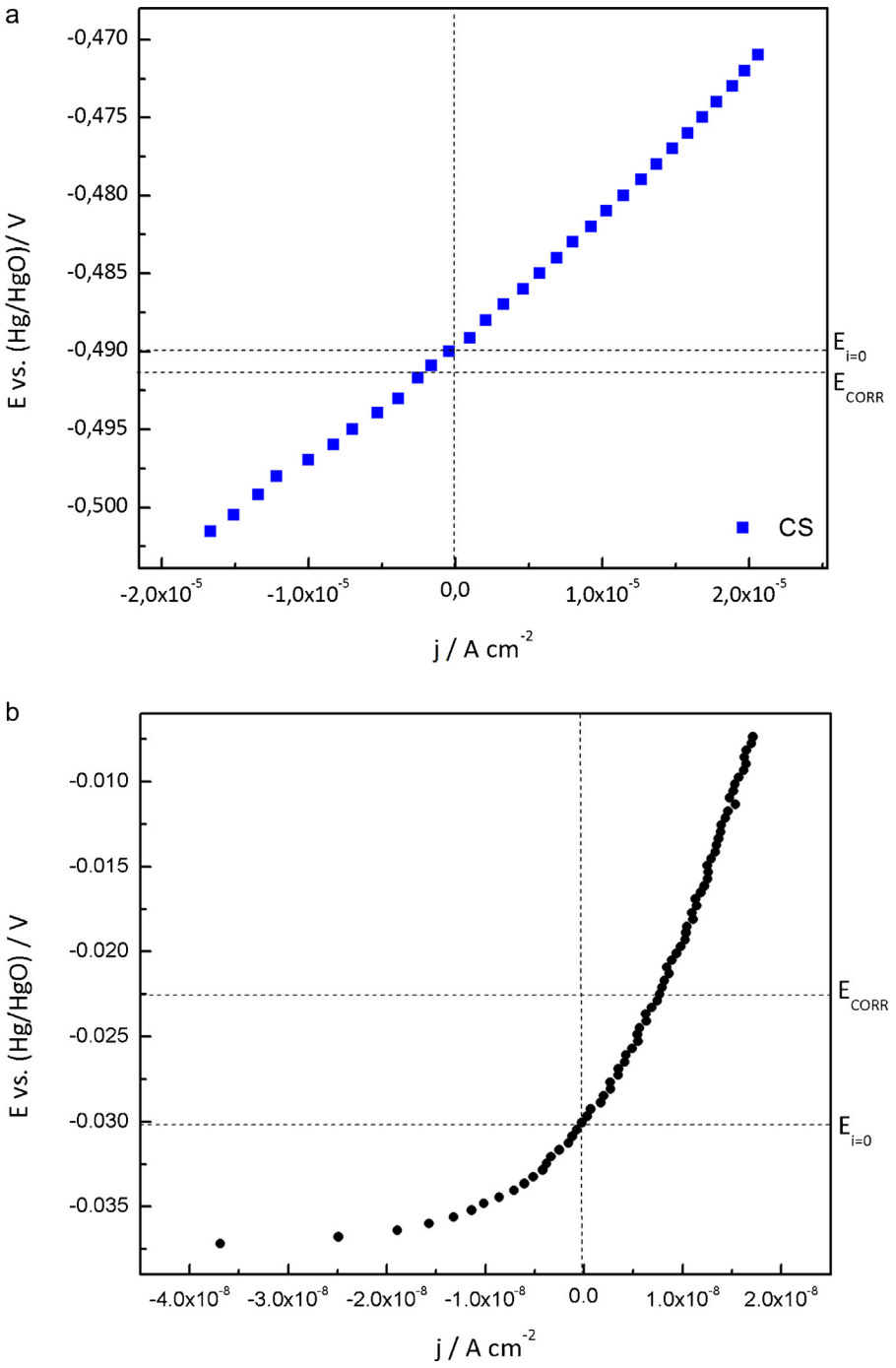

Fig. 3. Polarization curves obtained by sweeping the potential ± 15 mV from E_{corr} in a) CS (■) and b) IS100 (●). Sweep rate: 0.1 mV^{-1}.

E_{corr}, all of them calculated from at least three curves. The curve registered in CS confirms that steel is actively dissolving in CS. In contrast, a clearly different behavior can be seen when the inhibiting agent is present. A passive region, with a low *j*pas, can be identified. *j*pas is observed to decrease as the ratio $[HPO_4^{2-}]/[Cl^-]$ increases suggesting that a more compact film is present on the surface for the higher dosages of inhibitor. In the three ISs steel presents pitting. The pitting potential increases with the phosphate content. The difference E_{pit} - E_{corr} relates to the resistance to pitting [32]. Table 2 shows that E_{pit} - E_{corr} increases as the ratio $[HPO_4^{2-}]/[Cl^-]$ increases, in agreement with the presence of a surface film more resistant to pitting. However, repassivation is not observed in any of the dosages tested in agreement with the results from other authors [6]. Fig. 6 shows images of the electrodes after carrying out the polarization curves for CS and IS100. The images confirm uniform corrosion when phosphate ions are absent; just a stain appears on the metal surface. When phosphate ions are present, pits are observed.

Fig. 7 presents the cathodic polarization curves, after 24 h immersion in CS and IS100. In CS, three clearly delimited zones can be seen. Within region I oxygen reduction is under mixed control: activated and diffusion. In region II, the process is under diffusion control, with a limiting current reaching 6.45 10^{-5} A cm^{-2}. From -0.9 V onwards, in region III, water is decomposing. In the case of IS100, no

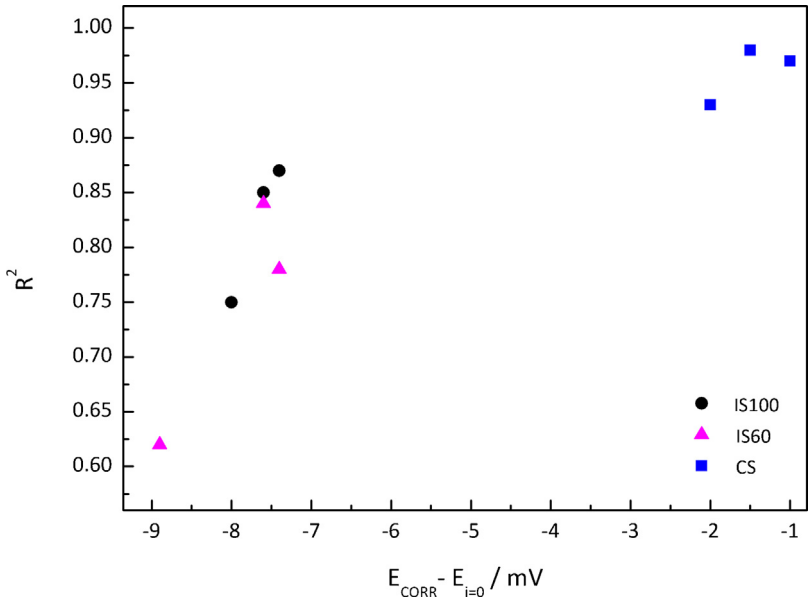

Fig. 4. The coefficient of determination R^2 plotted against the difference between the zero current potential ($E_{i=0}$) and the corrosion potential (E_{corr}). IS100 (●); IS60 (▲) and CS (■).

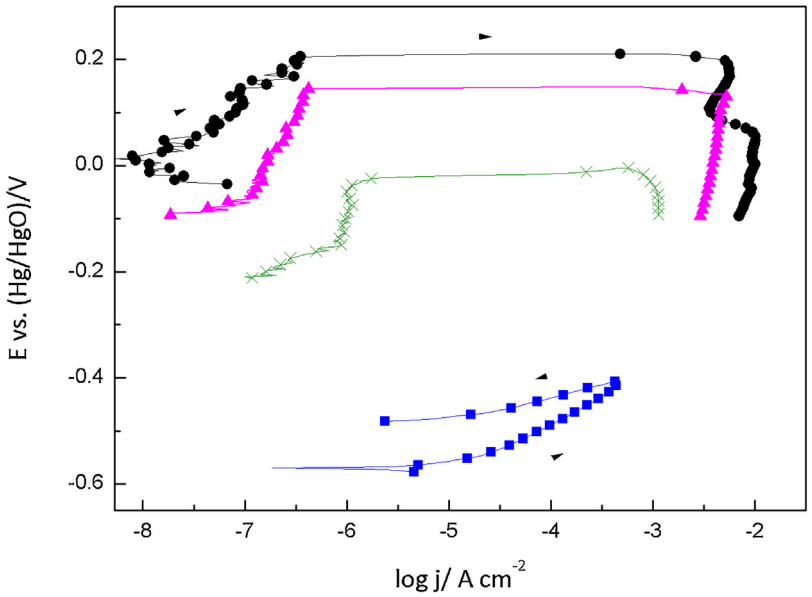

Fig. 5. Anodic polarization curves of steel after being 24 h at E_{corr} in CS (—■—), IS100 (—●—), IS60 (–▲–) and IS20 (–X–). Scan rate: 0.1 mV s^{-1}.

such defined zones can be observed. There is a peak in the curve most likely related to the simultaneous reduction of oxygen plus the reduction of the surface film formed during pretreatment. This superposition complicates the detection of a limited current. After the peak, from -0.6 V to more negative potential, the current is about one order of magnitude lower when the inhibiting agent is present.

Phosphates affect both the cathodic and the anodic currents in the polarization curves. However, the effect is related to the development of a passive film on the surface and results in a pronounced increment in E_{corr}. Therefore, this suggests that phosphates are behaving principally as anodic-type inhibitors in carbonated solutions contaminated with chloride ions.

Table 2
Relevant electrochemical parameters calculated from the anodic polarization curves shown in Fig. 5 and E_{corr} values measured after 24 at open circuit potential.

	E_{corr} vs. (Hg/HgO) / mV	E_{pic} vs. (Hg/HgO) / mV	E_{pic}-E_{corr}/mV	j_{pas}/μA cm^{-2}
CS	-498 ± 51	–	–	–
IS20	-238 ± 42	-9 ± 50	229 ± 54	9.7 ± 8
IS60	-91 ± 6	185 ± 49	276 ± 44	0.5 ± 0.04
IS100	-17 ± 7	268 ± 69	290 ± 55	0.3 ± 0.12

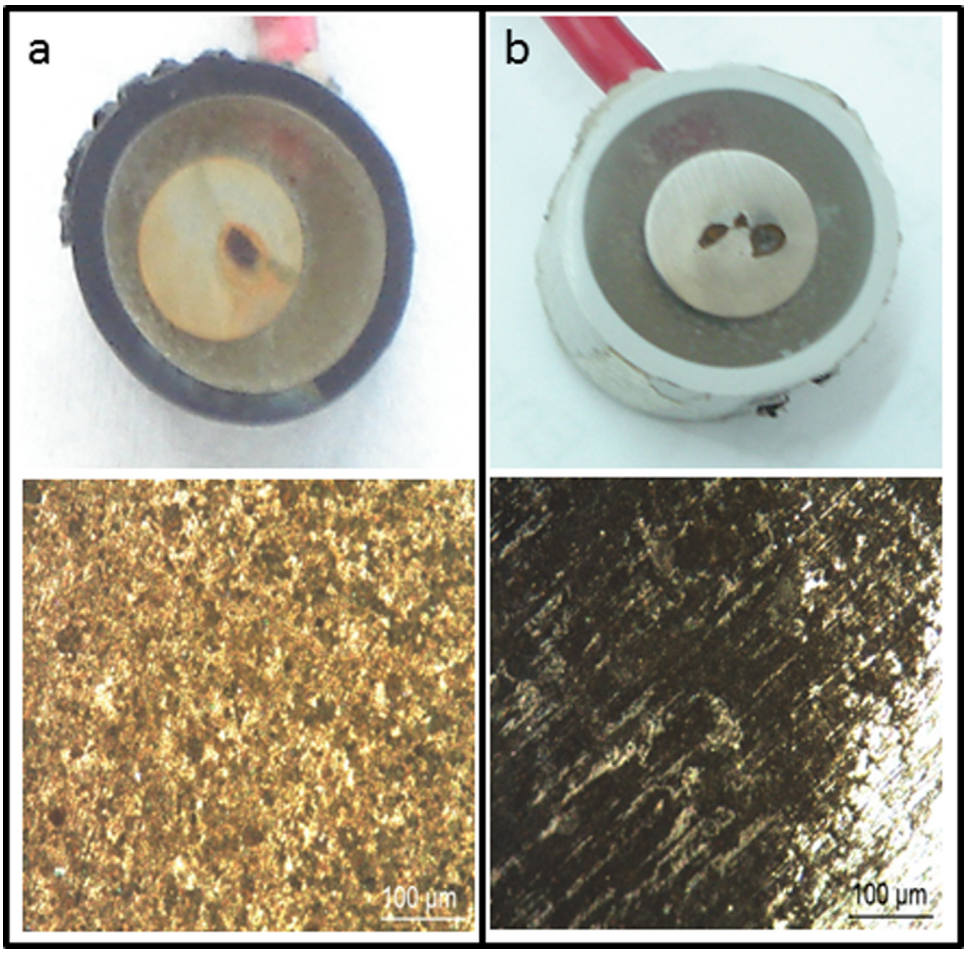

Fig. 6. Micrographs of electrodes after having carried out anodic polarization curves. a) CS and b) IS100.

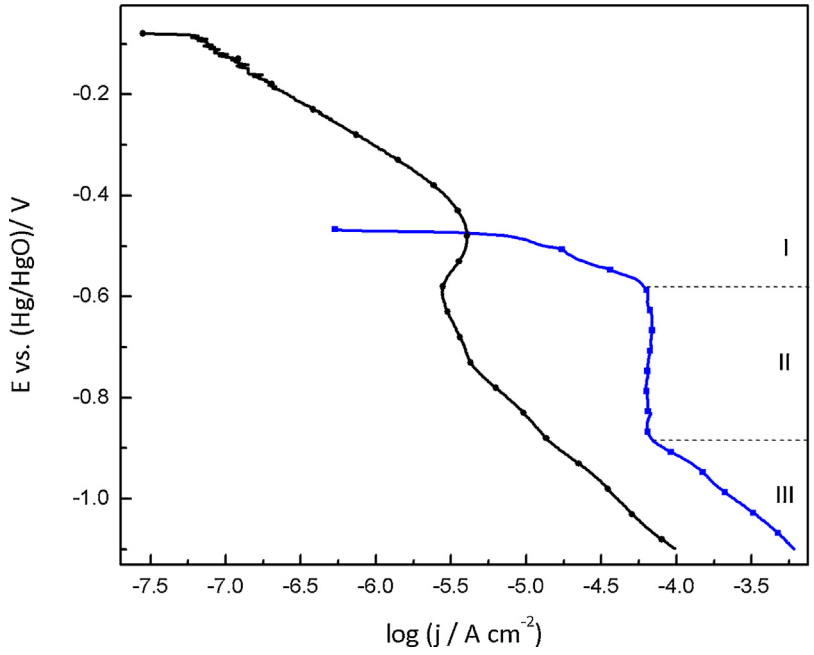

Fig. 7. Cathodic polarization curves of steel after being 24 h at E_{corr} in CS (—■—) and IS100 (—●—). Scan rate: 0.1 mV s^{-1}.

3.5. Electrochemical impedance spectroscopy

The impedance spectra recorded using electrodes aged during 24 hours in solutions with and without inhibiting agent are presented in Fig. 8a, b and c using Nyquist and Bode plots. Fitting curves to circuits in Fig. 1 are included in the graph and the fitting parameters are presented in Table 3.

Corroding electrodes are frequently modeled using constant phase elements (CPE) in the equivalent circuit. The impedance of this type of element can be defined using two parameters, Q and *n* as:

$$Z_{CPE} = [Q(j\omega)^n]^{-1} \quad (3)$$

where Q is a constant with dimensions of Ω^{-1} cm^{-2} s^n and *n* a constant power, with -1<*n*<1.

The experimental data can be reasonably fitted to the equivalent circuits proposed in Fig. 1. In the absence of inhibitor, the system can be represented by a Randles circuit. The pseudo capacitance and the charge transfer resistance present values that are typical of actively corroding steel [33]. R_t agrees well with the value shown in Table 1, calculated by lineal polarization. On the other hand, in the presence of inhibitor, two time constants can be identified in the Bode plot, suggesting a surface film that controls the corrosion process. In this condition, the results were fitted using the equivalent circuit in Fig. 1b. When the inhibitor is incorporated, Q_o and n_o do not present significant changes when the two inhibitor contents are compared (see Table 3). The similar values of Q_o (close to 50 $\mu\Omega^{-1}$ cm^2 s^n), together with n_0 values close to 0.9, can be related to a capacitive response, typical of a protective passive layer [12,19,34]. In parallel, R_o increases markedly when more inhibitor is incorporated indicating the development of a more compact and protective passive film. The values corresponding to the second time constant can be associated to the charge transfer reaction on the film/metal interface. Comparing the situation with and without inhibitor, a clear increment in the R_t values together with a decrease in Q_t in the presence of phosphate ions is evident. Metal dissolution

Table 3
Optmized values resulting from the fitting of the results in Fig. 8 to the circuits in Fig. 1.

	CS	IS60	IS100
R_s/Ω cm^2	32	15.8	13.0
$Q_o/\mu\Omega^{-1}$ cm^{-2}s^n	-	52.9	45.2
no	-	0.87	0.93
$R_o/k\Omega$ cm^2	-	37.0	356.0
$Q_t/\mu\Omega^{-1}$ cm^{-2} s^n	5200	35.4	13.1
nt	0.71	0.67	0.72
$R_t/k\Omega$ cm^2	1.5	925.1	1030

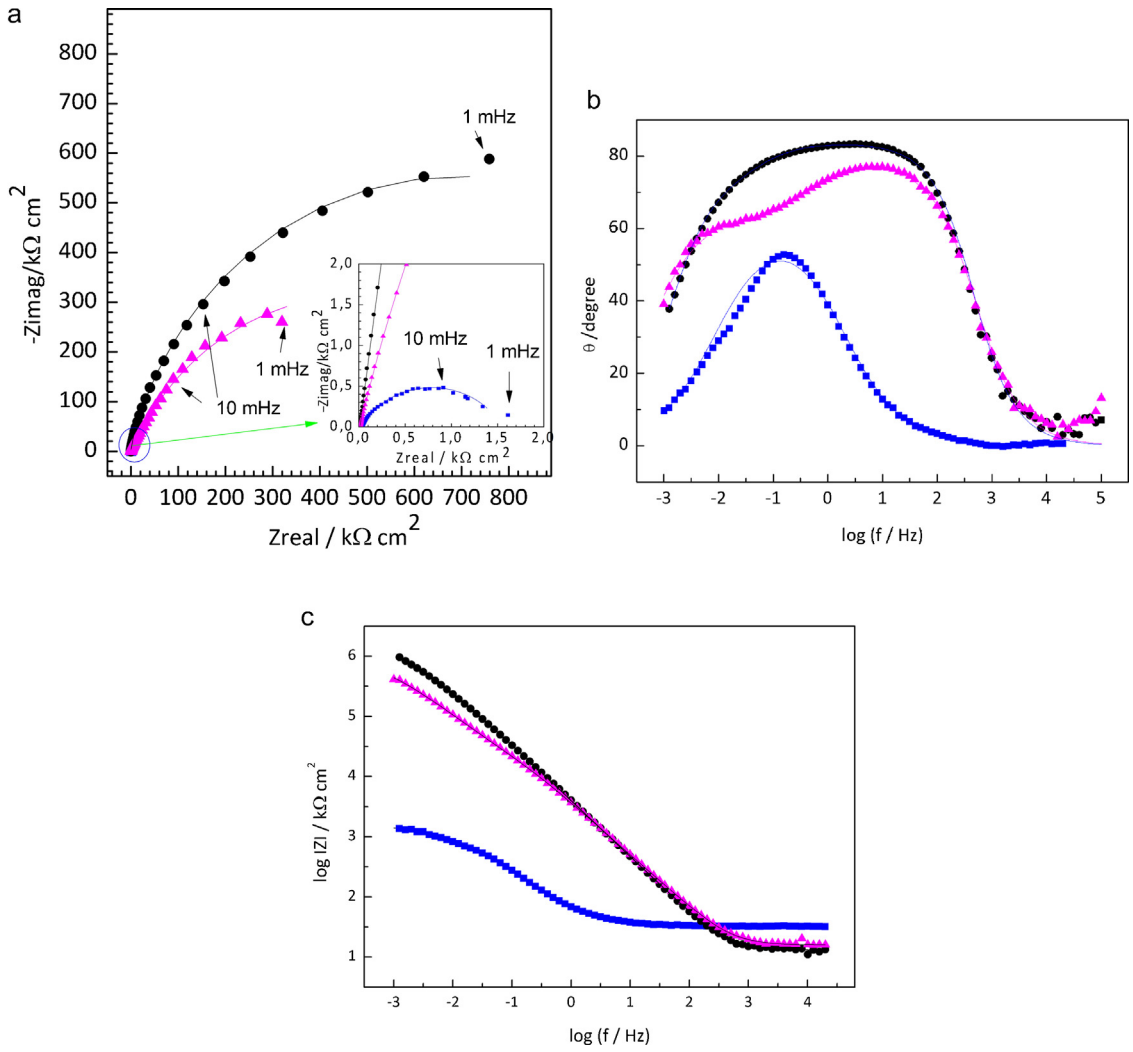

Fig. 8. Impedance spectra recorded on steel electrodes aged during 24 hours at E_{corr} in CS with and without inhibitor. The symbols represent the data and the lines the fitting results. (a) Nyquist representation; (b) and (c) Bode representation. CS (—■—), IS100 (—●—) and IS60 (—▲—).

sharply decreases when the inhibiting agent is present. The film becomes more protective as the biphosphate to chloride ratio approaches 1. Similar results were presented by Genin et al. [24].

3.6. Weight loss tests

Weight-loss tests were carried out by immersing steel coupons in each solution for 42 days. Fig. 9 shows photographs of the coupons after being removed from each electrolyte, as indicated. The corrosion current density values (i_{corr}) can be calculated from weight loss results using Faraday's law [35]

$$i_{corr} = \frac{\Delta m F}{A t eq} \quad (4)$$

where Δm is the mass lost, F is the Faraday constant, A is the exposed area, t is the exposure time and eq is the equivalent weight (Fe eq= 27.92 g/mol).

The percentage of inhibition was calculated using the following equation

$$\%\zeta = \left[1 - \frac{i_{\text{corr with inhibitor}}}{i_{\text{corr without inhibitor}}}\right] x100 \quad (5)$$

The results are shown in Table 4. As presented in Fig. 9, no attack was detected in the case of coupons immersed in IS100; weight loss is negligible. Also, the i_{corr} value in μA cm^{-2}, is typical of the passive state, even when the samples have been immersed for over one month. In contrast, corrosive attack is evident in every other case: CS, IS20 and IS60. Coupons immersed in CS showed generalized attack, with reddish and massive corrosion products. In turn, in contact with IS, localized attack is evident, which becomes more important as the inhibitor content decreases.

Table 4
Weight loss results after 42 days of immersion.

	Weight loss (mg)	Type of attack	% ζ	j_{corr} (μA cm^{-2})
CS	207.7	General	–	33.6
IS20	99.7	Pitting	52	16.1
IS60	14.6	Pitting	93	2.4
IS100	0.1	None	99.95	0.016

3.7. Raman confocal spectroscopy

Raman spectroscopy constitutes a useful tool to investigate the composition of surface films. Samples were analyzed after anodic polarization in IS100 and at the end of the weight loss tests in the different conditions. The results after anodic polarization curves are shown in Fig. 10. In this case, spectra were recorded on the corrosion products around pits (A) and on a clean zone (B) (see Fig. 6b). Spectrum (A) corresponds to the corroded region, where the presence of α-FeOOH can be detected by peaks located at 220, 280, 395 and 595 cm^{-1}. Between 940 and 1050 cm^{-1} phosphate can also be identified. These might be present as iron phosphates, as reported before in the literature [36–38]. The species HPO_4^{2-} presents characteristic signals at 850, 987 and 1080 cm^{-1} [38]. In turn, PO_4^{3-} shows its main peak between 900 and 1000 cm^{-1} which corresponds to the symmetrical stretch of the P-O bond.

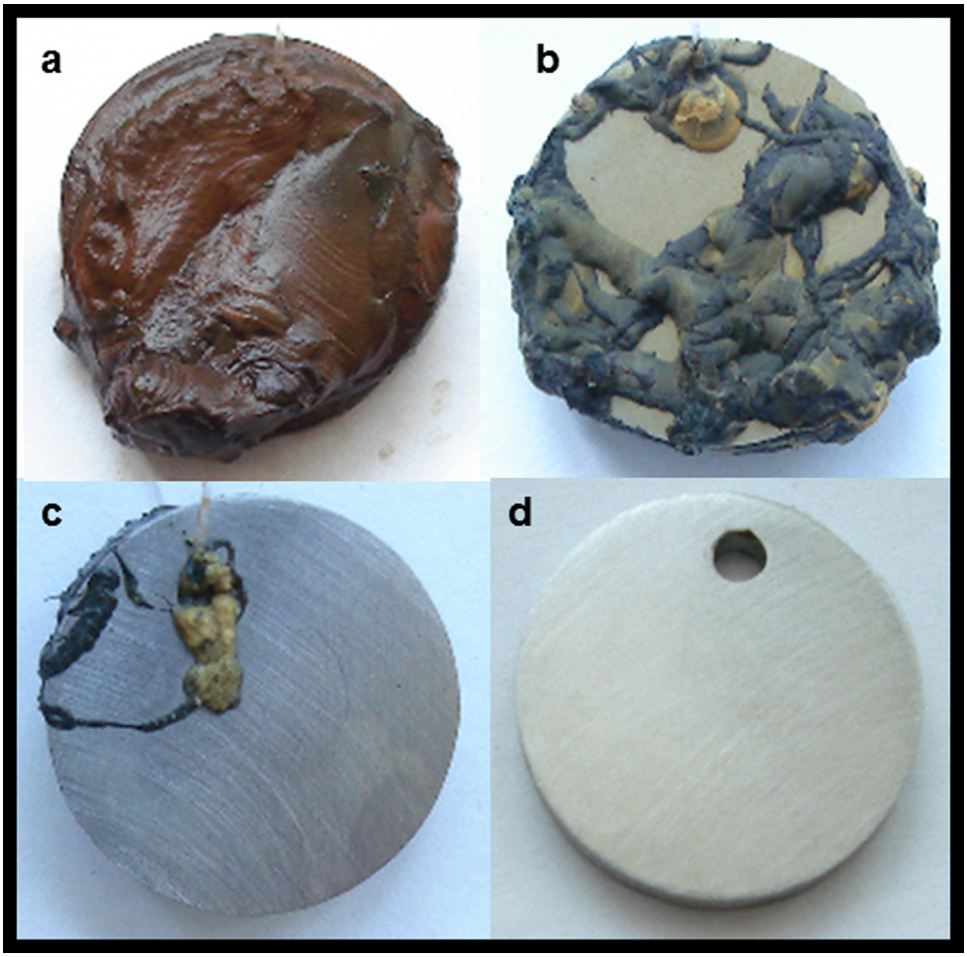

Fig. 9. Photographs of the coupons after a 42 days period of immersion in a) CS, b) IS20, c) IS60 and d) IS100.

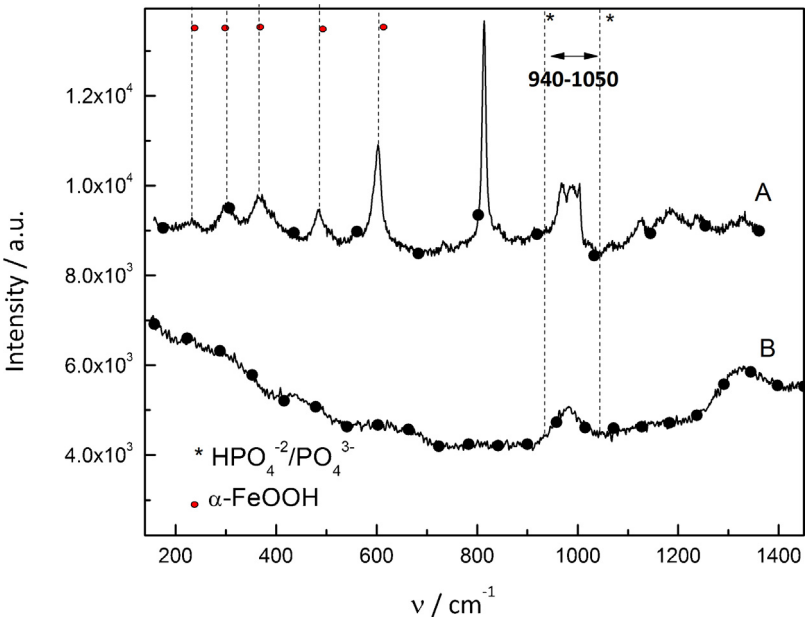

Fig. 10. Raman spectra of the steel surface after having carried out anodic polarization curves in IS100.

Furthermore, PO_4^{3-} shows three lower intensity peaks due to asymmetrical stretching between 900 and 1200 cm^{-1}. Spectrum (B) in Fig. 10 corresponds to the corrosion-free zone and presents a mostly featureless response. This behaviour suggests that a very thin film is present on the surface or also that the film is amorphous or a highly disordered mixture of iron oxides and oxo-hydroxides [37]. The broad band centred at 982 cm^{-1} suggests that phosphate ions are incorporated into the passive film.

Raman spectroscopy was also used to investigate the composition of the products formed on the steel surface after the 42 days immersion and prior to the cleaning process involved in the weight loss tests. Surface analysis was carried out on one coupon for each condition, surveying at least 5 different spots. The spectra are

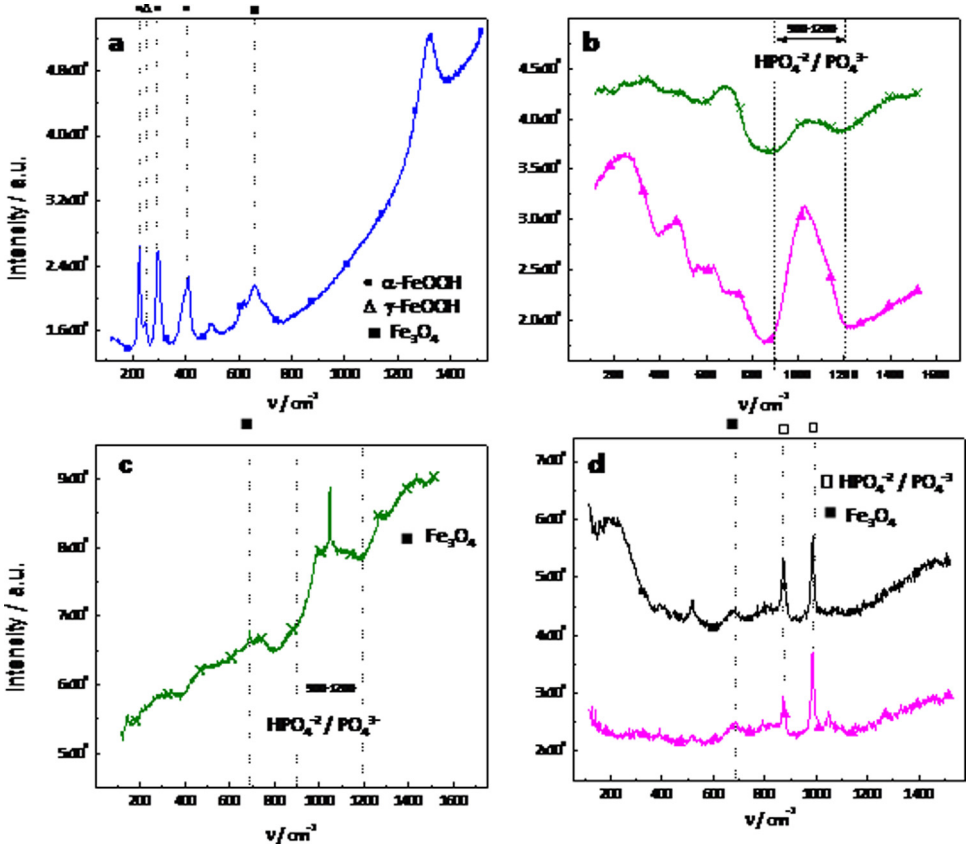

Fig. 11. Raman spectra on steel surface after a 42 days period of immersion. Corrosion products formed in a) CS (—■—); b) IS20(–X–) and IS60 (–▲–). Passive film in c) IS20 (–X–); d) IS60 (–▲–) and IS100 (—●—).

presented in Fig. 11. Graph **a** shows a representative spectrum of the sample immersed in CS and reveals the presence of α and γ-FeOOH. α-FeOOH displays bands at 220, 280 and 395 cm^{-1}, while the signal from γ-FeOOH can be seen at 245 cm^{-1}. Magnetite could be responsible for the peak located at 680 cm^{-1} [37,39].

It is well known that the products formed on the surface of steel depend on the composition of the solution. Several authors have observed the formation of *green rust*(GR) as intermediate transient compounds between $Fe(OH)_2$ and Fe(III) oxyhidroxides [6,38,40,41]. This is composed by Fe^{2+} and/or Fe^{3+} together with OH^-, Cl^- and CO_3^{2-}. These can form variations of GR such as GR-Cl^- ($3Fe(OH)_2{\cdot}Fe(OH)_2Cl{\cdot}nH_2O$) and/or GR-$CO_3^{2-}$ ($4Fe(OH)_2{\cdot}Fe_2(OH)_4CO_3{\cdot}nH_2O$) which can later be oxidized to α or γ-FeOOH [24,41].

$$Fe(OH)_2 \rightarrow GR \rightarrow \alpha \text{ or } \gamma\text{-FeOOH} \quad (5)$$

Refait et al. [41] concluded that no GR-CO_3^{2-} is formed when phosphates are simultaneously present with Fe^{2+}, OH^- and HCO_3^-. Graph **b** in Fig. 11 shows spectra of the green products found after prolonged immersion in IS20 and IS60. The band between 900-1200 cm^{-1} could be attributed to an amorphous layer of corrosion products that could include phosphate [42,43], as detailed above when discussing Fig. 10. The two spectra in Fig. 11b show bands with different intensities, in agreement with the differences in that visual aspect presented in Fig. 9. The spectra shown in Fig. 11(c) and (d) were taken from the passive zones (free of corrosion products) of IS20, IS60 and IS100. They are not superimposed because the intensity is much higher for IS20. This fact alone suggests that a thicker film has been formed when iron is in contact with IS20. All three spectra show the presence of magnetite (680 cm^{-1}). Also, between 900-1200 cm^{-1} the presence of the signal typical of phosphates provides evidence of this inhibitor being incorporated to the surface film.

3.8. X-ray photoelectron spectroscopy (XPS)

XPS spectra were recorded on samples kept for 192 h immersed in each solution. In every case, peak C1s (**B.E.**: 284.5 eV [44]) was taken as reference to correct the binding energy of the rest of the peaks. Fig. 12 presents the results for the surface films grown in IS100, where peaks corresponding to $Fe2p_{3/2}$, O1s and P2p are shown. Similar results were obtained for steel in contact with IS20 and IS60. The parameters obtained from deconvoluting the different signals are summarized in Table 5. In every spectra, the $Fe2p_{3/2}$ peak contains contributions from Fe^0, Fe(II) and Fe(III) [45,46]. The contribution from Fe^0 suggests that the thickness of the surface film is lower than 10 nm, as this is the maximum depth that can be evaluated by this technique [34,47]. The amount of Fe^0 increases with the ratio $[HPO_4^{2-}]/[Cl^-]$, which might suggest a thicker film for $[HPO_4^{2-}]/[Cl^-]$=0.2. Table 6 shows Fe^{III}/Fe^{II} and Fe^{0X}/Fe^{M} ratios, calculated from the analysis of XPS peaks. Fe^{0X}/Fe^{M} describes the amount of Fe II and III oxides formed, relative to the

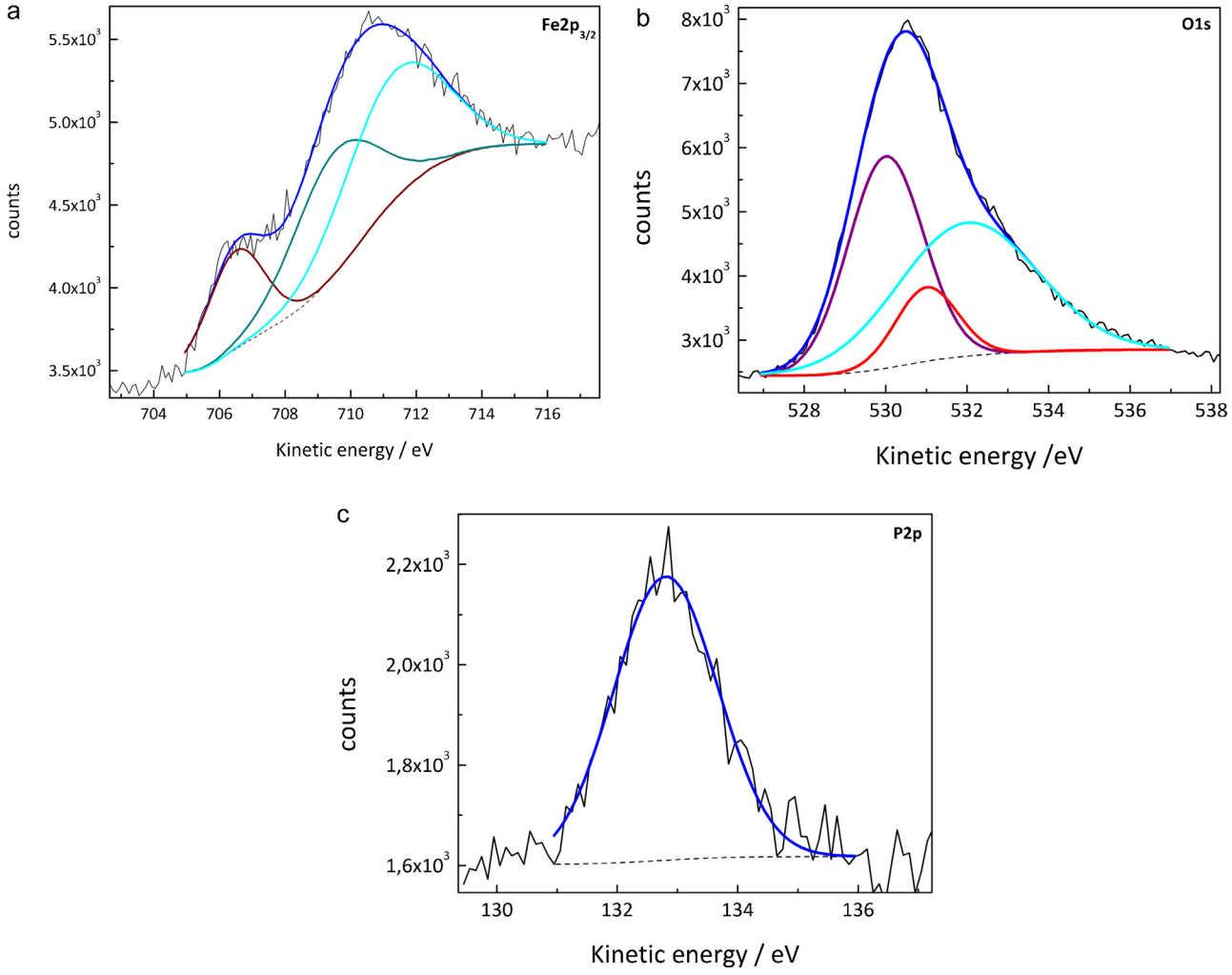

Fig. 12. XPS spectra for passive layers grown on steel for 192 h at E_{corr} in IS100. a); b) O1s; c) P2p.

Table 5
Characteristic parameters associated to the elements present on the surface film.

Condition	Peak	Component	Binding energy/eV	FWHM/eV	Atomic composition %
IS20	$Fe2p_{3/2}$	Fe^0	706.7	1.9	13.8
		Fe(II)	709.6	2.7	35.4
		Fe(III)	711	3.9	50.8
	O1s	O^{-2}	530	2.7	53
		OH^-	531	3	18.7
		HPO_4^{-2}	532	3.7	28.3
IS60	$Fe2p_{3/2}$	Fe^0	706.7	2	21
		Fe(II)	709.6	3	38.6
		Fe(III)	711	3.6	40.4
	O1s	O^{-2}	530	2.4	75.9
		OH^-	531	3.4	0.9
		HPO_4^{-2}	532	3.3	24.1
IS100	$Fe2p_{3/2}$	Fe^0	706.7	2	19.3
		Fe(II)	709.6	2	35.5
		Fe(III)	711	3.7	45.2
	O1s	O^{-2}	530	2.2	40.9
		OH^-	531	1.8	11.6
		HPO_4^{-2}	532	4	47.5

Table 6
Fe^{III}/Fe^{II} and Fe^{0X}/Fe^{M} ratios, calculated from the analysis of XPS peaks.

Sample	Fe^{III}/Fe^{II}	Fe^{0X}/Fe^{M}
IS20	1.43	6.24
IS60	1.10	3.76
IS100	1.27	4.18

amount of Fe^0 (metallic iron, Fe^M). Fe^{0X} is estimated by adding the contribution from Fe(II) and Fe(III) peaks in Fig. 12a [45]. The highest Fe^{0X}/Fe^M ratio was found for IS20, while the results for IS60 and IS100 are lower and similar. These facts suggest that more corrosion products are being formed for the lowest dosage of inhibitor. The Fe^{III}/Fe^{II} ratio is similar for the three conditions.

As regards the O1s peak, the three inhibitor dosages present contributions from O^{2-}, OH^- and PO_4^{3-}. The higher amount of HPO_4^{2-} was found when $[HPO_4^{2-}]/[Cl^-]$=1, where 47.5% of the O1s signal comes from HPO_4^{2-}. A higher incorporation of phosphate to the surface film could be associated to a more protective film. In turn, peak P2p (B.E.: 132.5 eV) [44] confirms that phosphorus is incorporated as phosphate in agreement with previous publications [6,18].

4. Conclusions

A synthetic solution that simulates the electrolyte contained in the pores of carbonated concrete contaminated with chlorides has been used (CS). To evaluate the performance of phosphate ions as corrosion inhibitors, three biphosphate dosages were tested where $[inhibitor]/[Cl^-]$=0.2, 0.6 and 1 (IS).

As expected, steel in CS shows E_{corr} and Rp values that are typical of actively corroding metals.

When phosphate is incorporated, a passive behaviour is found, as shown by nobler E_{corr} values, non-linear Rp curves and EIS results. Ferrous phosphate precipitation could be responsible for these changes, as detected by Raman spectroscopy and XPS. Due to the low carbonation degree in IS100, Fe dissolution could be favored, followed by immediate precipitation of ferrous phosphate on the steel surface.

After 24 h at open circuit potential in contact with biphosphate ions, impedance spectra show two time constants with high Ro and Rt values, confirming the presence of a passive film that controls the corrosion process. This film becomes more protective in the case of IS100. Also, as the $[HPO_4^{2-}]/[Cl^-]$ ratio increases, so does the difference (E_{pic}-E_{corr}), which proves a better resistance to localized attack for the highest inhibitor dosage. However, no repassivation was detected.

After over one month in immersion, steel remains passive in the condition IS100, with an inhibition factor higher than 99%. In contrast, in the case of IS60 and IS 20, pitting was detected.

Acknowledgments

This work has been supported by the University of Mar del Plata (Grant 15/G391), as well as by the National Research Council (CONICET, PIP0670). L. Yohai wishes to thank CONICET, Argentina, for her fellowship.

References

[1] M. Moreno, W. Morris, M.G. Alvarez, G.S. Duffo, Corrosion of reinforcing steel in simulated concrete pore solutions effect of carbonation and chloride content, Corrosion Science 46 (2004) 2681.
[2] W. Morris, M. Vázquez, Corrosion of reinforced concrete exposed to marine environment, Corrosion Reviews 20 (2002) 469–508.
[3] L. R. Liu, J. Jiang, C. Xu, Z. Song Xiong, Influence of carbonation on chloride-induced reinforcement corrosion in simulated concrete pore solutions, Construction and Building Materials 56 (2014) 16–20.
[4] C.-Q. Ye, R.-G. Hu, S.-G. Dong, X.-J. Zhang, R.-Q. Hou, R.-G. Du, C.-J. Lin, J.-S. Pan, EIS analysis on chloride-induced corrosion behavior of reinforcement steel in simulated carbonated concrete pore solutions, Journal of Electroanalytical Chemistry 688 (2013) 275–281.
[5] S. Fajardo, D.M. Bastidas, M. Criado, J.M. Bastidas, Electrochemical study on the corrosion behaviour of a new low-nickel stainless steel in carbonated alkaline solution in the presence of chlorides, Electrochimica Acta 129 (2014) 160–170.
[6] M. Reffass, R. Sabot, M. Jeannin, C. Berziou, P. Refait, Effects of phosphate species on localised corrosion of steel in $NaHCO_3$ + NaCl electrolytes, Electrochim. Acta 54 (2009) 4389–4396.
[7] Q. Pu, L. Jiang, J. Xu, H. Chu, Y. Xu, Y. Zhang, Evolution of pH and chemical composition of pore solution in carbonated concrete, Construction and Building Materials 28 (2012) 519–524.
[8] J.M. Gaidis, Chemistry of corrosion inhibitors, Cement & Concrete Composites 26 (2004) 181.
[9] C.M. Hansson, L. Mammoliti, B.B. Hope, Corrosion inhibitors in concrete. Part I: the principles, Cem. Concr. Compos. 28 (1998) 1775–1781.
[10] T.A. Söylev, M.G. Richardson, Corrosion inhibitors for steel in concrete: state of the art report, Constr. Build. Mater 22 (2008) 609.
[11] M. Saremi, E. Mahallati, A study on chloride-induced depassivation of mild steel in simulated concrete pore solution, Cem. and Conc. Res. 32 (2002) 1915–1921.
[12] M.B. Valcarce, M. Vázquez, Carbon steel passivity examined in solutions with a low degree of carbonation: The effect of chloride and nitrite ions, Mater. Chem. Phys. 115 (2009) 313–321.
[13] L. Yohai, M. Vázquez, M.B. Valcarce, Phosphate ions as corrosion inhibitors for reinforcement steel in chloride-rich environments, Electrochimica Acta 102 (2013) 88–96.
[14] S.M. Abd El Haleem, S. Abd El Wanees, E.E. Abd El Aal, A. Diab, Environmental factors affecting the corrosion behavior of reinforcing steel II. Role of some

anions in the initiation and inhibition of pitting corrosion of steel in $Ca(OH)_2$ solutions, Corrosion Science 52 (2010) 292–302.
[15] H. Nahali, L. Dhouibi, H. Idrissi, Effect of phosphate based inhibitor on the threshold chloride to initiate steel corrosion in saturated hydroxide solution, Construction and Building Materials 50 (2014) 87–94.
[16] J.J. Shi, W. Sun, Effects of phosphate on the chloride-induced corrosion behavior of reinforcing steel in mortars, Cement and Concrete Composites 45 (2014) 166–175.
[17] N. Etteyeb, L. Dhouibi, H. Takenouti, M.C. Alonso, E. Triki, Corrosion inhibition of carbon steel in alkaline chloride media by Na3PO4, Electrochim. Acta 52 (2007) 7506–7512.
[18] Z. Szklarska-Smialowska, R.W. Staehle, Ellipsometric study of the formation of films on iron in orthosphosphate solutions, J Electrochem Soc 121 (1974) 1393–1401.
[19] M.B. Valcarce, M. Vázquez, Carbon steel passivity examined in alkaline solutions: The effect of chloride and nitrite ions, Electrochim. Acta 53 (2008) 5007–5015.
[20] ZPlot for Windows Scribner Associates Inc. 1998.
[21] X. X. Mao, R.W. Revie Liu, Pitting corrosion of pipeline steel in dilute bicarbonate solution with chloride ions, Corrosion 50 (1994) 651–657.
[22] M. Pourbaix, Atlas of Electrochemical Equilibrium in Aqueous Solutions, Pergamon Press, Oxford (1966) 307.
[23] M.J. Pryor, M. Cohen, The inhibition of corrosion of iron by some anodic inhibitors, Journal of Electrochemical Society 100 (1953) .
[24] J.M.R. Génin, L. Dhouibi, P. Refait, M. Abdelmoula, E. Triki, Influence of phosphate on corrosion products of iron in chloride-polluted-concrete-simulating solutions: Ferrihydrite vs green rust, Corrosion 58 (2002) 467–478.
[25] L.J. Simpson, C.A. Melendres, Surface-enhanced Raman spectroelectrochemical studies of corrosion films on iron in aqueous carbonate solution, J. Electrochem. Soc. 143 (1996) 2146–2152.
[26] M.C. Alonso, M.C. Andrade, The electrochemical behaviour of steel reinforcements in Na_2CO_3 and $NaHCO_3$ solutions in relation to stress corrosion cracking, Corros. Sci. 29 (1989) 1129–1139.
[27] X. X. Mao, R.W. Revie Liu, Pitting corrosion of pipeline steel in dilute bicarbonate solution with chloride ions, Corrosion 50 (1994) 651–657.
[28] D.A. Jones, Principles and prevention of corrosion-2nd, Prentice-Hall Inc., 1996.
[29] F. Mansfeld, M., Fontana, R. Staehle, The polarization resistance technique for measuring corrosion currents., Plenum press, New York, 1976, pp. 163-253.
[30] M. Kouřil, P. Novák, M. Bojko, Limitations of the linear polarization method to determine stainless steel corrosion rate in concrete environment, Cem Concr Compos 28 (2006) 220–225.
[31] J.A. Gonzalez, A. Molina, M.L. Escudero, C. Andrade, Corros. Sci. 25 (1985) 917–930.
[32] Y. Feng, W.K. Teo, K.S. Siow, K.L. Tan, A.K. Hsieh, The corrosion behaviour of copper in neutral tap water. Part I: Corrosion mechanism, Corrosion Science 38 (1996) 369–385.
[33] M.B. Valcarce, C. Lopez, M. Vazquez, The Role of Chloride, Nitrite and Carbonate Ions on Carbon Steel Passivity Studied in Simulating Concrete Pore Solutions, Journal of the Electrochemical Society 159 (2012) C244.
[34] K. W. Xu, X. Daub, J.J. Zhang, D.W. Noel, J.C. Wren Shoesmith, Oxide formation and conversion on carbon steel in mildly basic solutions, Electrochim. Acta 54 (2009) 5727–5738.
[35] American Society of Testing and Materials, ASTM G102-89, Standard Practice for Calculation of Corrosion Rates and Related Information from Electrochemical Measurements, Philadelphia, 1994.
[36] R.L. Frost, An infrared and Raman spectroscopic study of natural zinc phosphates, Spectrochim. Acta Part A Mol. Biomol. Spectrosc. 60 (2004) 1439–1445.
[37] B. Diaz, S. Joiret, M. Keddam, X.R. Nóvoa, M.C. Pérez, H. Takenouti, Passivity of iron in red mud's water solutions, Electrochim. Acta 49 (2004) 3039–3048.
[38] S. Simard, M. Odziemkowski, D.E. Irish, L. Brossard, H. Ménard, In situ micro-Raman spectroscopy toinvestigate pitting corrosion product of 1024 mild steel in phosphate and bicarbonate solutions containing chloride and sulfate ions, J. Appl. Electrochem. 31 (2001) 913–920.
[39] A. Hugot-Le Goff, J. Flis, N. Boucherit, S. Joiret, J. Wilinski, Use of Raman spectroscopy and rotating split ring disk electrode for identification of surface layers on iron in 1M NaOH, J. Electrochem. Soc. 137 (1990) 2684–2690.
[40] M. Jeannin, D. Calonnec, R. Sabot, P. Refait, Role of a clay sediment deposit on the passivity of carbon steel in 0.1mol dm^{-3} $NaHCO_3$ solutions, Electrochimica Acta 56 (2011) 1466–1475.
[41] P. Refait, M. Reffass, J. Landoulsi, R. Sabot, M. Jeannin, Role of phosphate species during the formation and transformation of the Fe(II-III) hydroxycarbonate green rust, Colloids Surf. A Physicochem. Eng. Asp. 299 (2007) 29–37.
[42] D.L.A. De Faria, S. Venâncio Silva, M.T. De Oliveira, Raman microspectroscopy of some iron oxides and oxyhydroxides, J. Raman Spectrosc. 28 (1997) 873–878.
[43] L.J. Simpson, C.A. Melendres, Temperature dependence of the surface enhanced raman spectroelectrochemistry of iron in aqueous solutions, Electrochimica Acta 41 (1996) 1727–1730.
[44] J.F. Moulder, J. Chastain, Handbook of X-ray Photoelectron Spectroscopy: A Reference Book of Standard Spectra for Identification and Interpretation of XPS Data, 1995, pp. 261.
[45] P. Ghods, O.B. Isgor, J.R. Brown, F. Bensebaa, D. Kingston, XPS depth profiling study on the passive oxide film of carbon steel in saturated calcium hydroxide solution and the effect of chloride on the film properties, Appl. Surf. Sci. 257 (2011) 4669–4677.
[46] M.C. L.Q. Guo, L.J. Lin, A.A. Volinsky Qiao, Duplex stainless steel passive film electrical properties studied by in situ current sensing atomic force microscopy, Corros. Sci. 78 (2014) 55–62.
[47] B. Huet, V. L'Hostis, F. Miserque, H. Idrissi, Electrochemical behavior of mild steel in concrete: Influence of pH and carbonate content of concrete pore solution, Electrochimica Acta 51 (2005) 172–180.